

# NOVEL L-SHAPED GURNEY FLAP FOR ROTORCRAFT VIBRATION REDUCTION

V. Motta\*, G. Quaranta\*

\*Dipartimento di Scienze e Tecnologie Aerospaziali – Politecnico di Milano  
Campus Bovisa, Via La Masa 34, 20156 Milano – Italy  
e-mail: valentina.motta@polimi.it

## Abstract

This work concerns an assessment of the rotor blade vibration reduction capabilities of a novel L-shaped trailing edge Gurney Flap. The primary effect of this L-tab is represented by a modification of the reference airfoil mean line shape, both in terms of camber and chord length, this latter being related to the two counter rotating vortical structures developed past the tab vertical prong. Previously validated computational fluid dynamics results are exploited to develop a physically based thin-line reduced order model, which successfully reproduces the mean line modifications induced by the L-tab, in addition to accurately capture the steady aerodynamic forces and the first harmonic of the unsteady loads generated by fixed configurations of the airfoil L-tab system and by oscillating motions of the movable device. A thin-line linear model is also developed for a blade section equipped with a classical trailing edge flap. Comparisons of the aerodynamic loads generated by these two movable devices for equal input oscillation laws, allow to estimate the ranges of reduced frequency where the L-tab is expected to perform better with respect to the trailing edge flap and vice-versa. These two reduced order models are then exploited to build up two separate three degrees of freedom linear aerostructural models for a blade equipped with a partial span L-tab or a trailing edge flap. A higher harmonic control algorithm is then applied and compared between the two devices to reduce separately the  $N/\text{rev}$  harmonics of the blade root rotating frame vertical force, flapping and feathering moments. A significant reduction of the vibratory loads is obtained. Moreover, the attainment of similar results with a well known trailing edge device, such the classical flap taken under consideration, is a further confirmation of the potential feasibility of this novel L-tab as an effective alternative mean for vibration reduction on rotor blades.

## 1. INTRODUCTION

The Gurney Flap (GF) was originally designed for the race car of Dan Gurney to increase the vehicle downforce generated by the rear inverted wing [1]. Since then, the GFs have also attracted much attention of aircraft and rotorcraft designers as a very effective high-lift device. Moreover, GFs are successfully applied in wind turbines and in turbomachinery.

The GF effectiveness stems directly from its extreme simplicity: a flat edge attached to the Trailing Edge (TE) and perpendicular to the chord line.

On the contrary, classical high lift devices are very complex, both in terms of aerodynamics that governs their functioning, and of mechanical systems necessary to activate them, requiring a high level of maintenance operations. Liebeck [2] was among the first to study the behavior of Gurney flaps for aeronautical applications. On the basis of his experimental studies, he found that two counter rotating vortices are generated behind the Gurney flap, since the flow is forced to turn around the perpendicular plate at the TE. The intersection point of the streamlines coming from the pressure and from the suction side, is shifted away from the TE.

As a consequence, the location of the Kutta condition is shifted downstream the TE, resulting in a net effect in terms of load that is equivalent to what can be obtained by a longer effective chord and a more cambered airfoil. The interpretation proposed by Liebeck in Ref. [2] on the aerodynamic effects of GFs was confirmed by later studies. Experiments conducted on airfoils equipped with GFs highlighted the capability of these devices to significantly increase lift without severe drawbacks in terms of drag increment [3–10]. Several numerical computations were also performed to investigate the behavior of GFs [9, 11–15]. These studies highlighted how such movable devices allow to increase the lift, and in particular the maximum lift, and the lift to drag ratio.

Recently, large interest was directed toward movable aerodynamic surfaces for aerodynamic performance improvement, alleviation of vibratory loads, flutter suppression and modification of the vortical wake. Several authors worked on the application of movable trailing edge flaps on rotorcraft blades for vibratory load control, see Refs. [16–20], and for the mitigation of negative effects associated with dynamic stall, see Refs. [21–23]. Since a GF has considerably less inertia than a traditional flap, smaller forces are expected to be required to actuate the system. As a consequence, a larger bandwidth can be achieved together with a reduced modification of the structural stiffness of the blades. Gerontakos and Lee [24] performed experimental measurements on a NACA 0012 section equipped with fixed GF like strips both on the pressure and on the suction side of the airfoil. They showed that trailing edge strips are suitable to improve performance of oscillating airfoils, in dynamic stall conditions. Tang and Dowell [25] validated a numerical model of a fixed GF on an oscillating airfoil, against the the experiments of Ref. [24]. Then, they showed through numerical computations that an oscillating Gurney flap brings additional benefits for deep-stall cases. Moreover, in Ref. [26] they carried out experiments on an oscillating NACA 0012 equipped with an oscillating GF, reaching the same conclusions of the numerical work, i.e., that an oscillating small strip located near the trailing edge can be used for active aerodynamic flow control of a wing.

An interesting application of GF like devices on rotorcraft, which is indeed the aim of the present study, concerns the alleviation of vibratory loads. Kinzel et al. [27] performed several steady and unsteady numerical simulations for various flow conditions over a S903 section equipped with GFs,

referred to as Miniature Trailing edge Effectors (MiTEs). Such simulations gave an overview on the possible usage of MiTEs both to improve performance and to reduce vibratory loads on helicopter blades. Additionally, they investigated the effect of chordwise positioning of the GF, showing that increased upstream positioning enlarges the hysteresis loop, degrades the lift enhancement, increases drag and decreases the nose-down pitching moment. Similar limits were found also in Refs. [10, 14, 28, 29]. Matalanis et al. [30] carried out 2D and 3D simulations, together with experimental measurements, on a VR-12 section equipped with a deployable GF. They investigated the effects of the actuation frequency of the movable device on the vibratory moment coefficient, showing, by Computational Fluid Dynamics-Computational Structural Dynamics (CFD-CSD) coupled analyses on a model of the UH-60A, that significant reduction of vibratory loads can be achieved. Min et al. [31] by using CFD-CSD simulations, found significant vibration reduction on the classical HART-II [32] test case with deployable GF. Liu et al. [33] investigated by numerical simulations the effect of several Gurney flap like devices on a NACA 0012 airfoil. They used numerical CFD computations as a reference to develop a Reduced Order Model (ROM) for the unsteady loads developed by the airfoil section equipped with this movable device. This model was used within a comprehensive solver, and an active control system was designed to effectively reduce vibratory loads on a helicopter rotor.

Despite the progress in the understanding the behavior of these movable devices, the integration of an active GF on a helicopter blade is still a very challenging design problem. In particular, it is necessary to stow the deployable device, together with the actuation mechanism, at the TE, complying with weight and balance constraints related to the aeroelastic behavior of the blades. Moreover, classical sliding actuation solutions, widely used for fixed wing GFs, are likely to undergo failures, under large centrifugal loads as those affecting rotor blades. Palacios et al. [34] carried out several experimental tests to investigate the operation of MiTEs under centrifugal forces comparable to those encountered on rotor blades. They found that indeed such devices are capable to effectively operate in these conditions. Moreover the estimated power requirements of GF like devices were found significantly lower than those of classical plain flaps. So, they proposed a concept of a novel pneumatic actuation system exploiting the pressure radial gradients within the rotor blades.

In an attempt to overcome stowage and actuation issues at the same time, Zanotti et al. [35, 36] proposed an L-shaped tab, i.e. a combination between a TE spoiler, namely a classical split flap, and a GF applied at the TE of a helicopter blade section. This concept has the additional advantage of locating the GF on the trailing edge, therefore maximizing its performance as shown in Refs. [10, 14, 27–29]. Experimental measurements carried out by Zanotti et al. [35, 36] showed that this novel L-shaped tab could be exploited both downward deployed, as a GF, and upward deflected, as a classical TE flap, to mitigate the negative effects of dynamic stall.

To verify the capabilities of this novel device also for the control of vibratory loads in flow conditions far from those of dynamic stall, the behavior of the unsteady loads due to oscillations of the airfoil and of the L-tab was investigated numerically, by means of CFD. A preliminary numerical assessment of the behavior of this device was reported in Ref. [15]. The analyses highlighted how the L-tab allowed the enhancement of performance, both for small and high angles of attack in steady state conditions. Additionally, simulations carried out for small amplitude pitch oscillations of the section equipped with such L-tab [37] showed the potential suitability of such device, both downward and upward deployed for vibration reduction on helicopter blades.

Although effective, these simulations are computationally expensive, and as such are not efficient during the design process and the development of control strategies. Thus, it is necessary to develop a ROM starting from CFD simulations. With this regard Liu and Montfort [38] proposed an analytical interpretation of steady effects of GFs on the basis of the thin airfoil theory. An extension of the thin-plate approach to the unsteady domain was proposed by Kinzel et al. [39]. The model was based on the formulation of Hariharan and Leishman [40], originally developed for airfoils equipped with a classical flap, and essentially it looks for an equivalent flap size which returns the indicial response that best approximates the indicial response of the GF obtained through a CFD computation. The formulation allows to keep into account the effects of the Mach number. These linear models are capable to capture the harmonic components of the aerodynamic loads. An extension was proposed in Ref. [41], to model also the non-harmonic disturbances visible in the results of CFD simulations.

A different approach was proposed by the au-

thors in a previous work [37], within the aim of developing a physically based linear ROM for the first harmonic component of the unsteady lift and moment. Such approach does not require to run a CFD indicial response simulation, but relies on physical flow features, such as the mean size of the Counter Rotating Vortices structures (CRV) developed past the L-tab discussed in this work. Notice that the correct representation of the first harmonic is the primary interest of the ROM in view of the application of Higher Harmonic Controls (HHC) for vibration reduction. The ROM was found capable to accurately reproduce the steady forces, as well as the first harmonic of the unsteady loads. Moreover the near-body flow field, including the inclination and the length of the CRV past the L-tab, is well captured by the equivalent geometry of the ROM.

The goal of this work is to assess the vibration reduction capabilities of the present L-tab, when installed on helicopter rotors, exploiting the aforementioned ROM to build up the aerodynamic transfer matrix of the aerostructural model for the blade. Moreover such thin-line based formulation is used to perform a comparison between the unsteady airloads generated by the L-tab under consideration and those developed by a classical trailing edge flap, both oscillating with the same law. Namely a two segments piece-wise mean line ROM is used to represent the airfoil equipped with the trailing edge flap. This comparison is carried out for several reduced frequencies, ranging from 0 up to 0.6. The HHC approach [42], is herein employed to compute proper control laws for the L-tab and the TE flap respectively, with the aim to reduce the blade root loads at one specific harmonic a time.

## 2. GEOMETRY AND REDUCED ORDER MODEL FOR A BLADE SECTION WITH THE L-TAB

Figure 1 shows a schematic view of the L-tab geometry positioned on the TE of the airfoil. The device resembles the one employed by Zanotti et al. [36] in their dynamic stall experiments.

The L-tab chordwise length is  $20\%c$ , while the height of its transverse prong is  $1.33\%c$ . The L-tab downward deflected protrudes  $1.01\%c$  from the airfoil pressure side, being the geometry of the clean airfoil cut before the trailing edge. This is consistent with the GF heights found in literature, that commonly range between  $0.5\%c$  to  $3\%c$  [8]. The L-tab is designed to be in rest position when is rotated upward by 4 degrees, measured starting

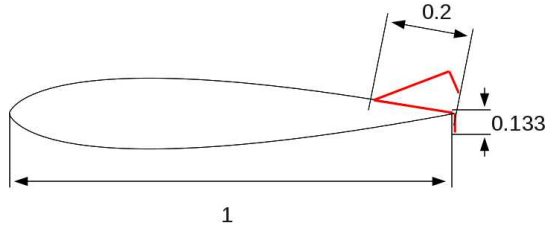


Figure 1: Schematic of the NACA 0012 section equipped with the TE L-tab.

from the position where the device is supported by the suction surface. In this condition the end of the vertical prong lies aligned with the suction side corner of the trailing edge. Therefore, the baseline configuration of the resulting airfoil presents a divergent TE. With this regard several experimental tests, see Refs. [43,44] shown that these divergent TE configurations could be effective especially for transonic flow conditions, being these latter not unusual for rotorcraft blade sections.

The development of a physically consistent ROM for the L-tab equipped NACA 0012 section is detailed in a previous work [37]. The main features of such ROM are briefly reported hereinafter for convenience. There are few studies on the physical mechanism of the GF lift enhancement, but there is a general agreement on the fact that the couple of CRV structures that appear in the flow behind the GF causes a shift of the trailing-edge Kutta condition [2] as shown in figure 2.

This vortical region on the trailing edge can be considered an extension of the airfoil that increases the effective chord and modifies the camber, resulting in the experienced lift and moment magnitude enhancement [8]. For subsonic flows the GF causes an increase of the pressure coefficient  $C_P$  along the entire airfoil. Analogous effects on the mean line shape are observed both experimentally and numerically for the L-tab herein considered [15,35–37,45]. An extended assessment of the steady and unsteady behavior of the L-tab installed on a NACA 0012 airfoil [15,37,45] is used as a reference for the development of the present ROM. With the aim to obtain a model capable to correctly capture the near body physics induced by the L-tab, the aforementioned mean line modifications have to be accurately reproduced. The analytical formulation of Küssner and Schwarz [46,47], suitable for arbitrarily shaped mean lines under the hypothesis of small perturbation, is used as benchmark for the ROM development. Notice that the small perturbation assumption is perfectly suitable

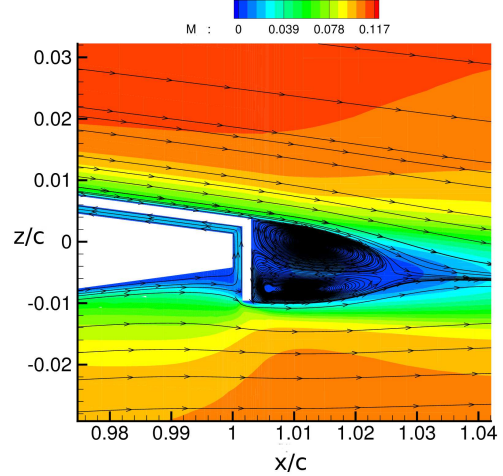


Figure 2: Mach number flow field and streamlines close to the trailing edge of the L-tab equipped blade section, resulting from CFD simulations; angle of attack = 0 degrees, freestream Mach number  $M = 0.117$ , Reynolds number  $Re = 1 \cdot 10^6$ .

for the ultimate goal of the present work, focused on the control of vibration on helicopter blades. Consistently with this assumption, the blade section with the movable L-tab is treated as a linear system with three Degrees Of Freedom (DOFs). These are namely pitch ( $\alpha$ ) and plunge ( $h/c$ ) oscillations of the airfoil, with the movable device in fixed position, and harmonic deflections of the L-tab ( $\beta$ , zero when downward deployed and positive for upward deflections), at constant angle of attack of the airfoil. A ROM is also derived for fixed configurations of the airfoil-tab system [37]. Notice that, for unsteady motions of the airfoil or of the L-tab, various reduced frequencies  $k = \omega c/2U$  in the range [0.1 0.6] are taken under consideration. It appears useful to remark that, since the present work concerns the small perturbation regime, a linear behavior of the system is expected when changing the parameters of the motion laws, both in terms of steady mean values and of oscillation amplitude.

The airfoil equipped with the L-tab is treated as a piecewise-linear thin-line, which represents the airfoil plus two movable surfaces: an aileron and a tab, see figure 3. The first segment represents the baseline airfoil, which can be either in fixed position or in harmonic pitch or plunge motions. The second segment is representative of the flap portion of the L-shaped GF and is referred to as Equivalent L-Tab (ELT). The third segment represents the effect of the CRV developed by the L-tab and it extends beyond the trailing edge of the airfoil. This

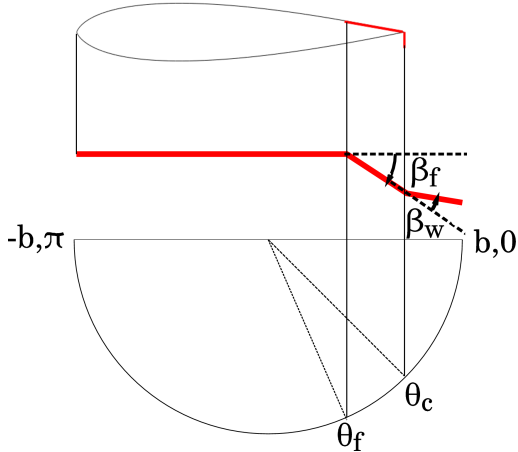


Figure 3: Mean line geometry and identification parameters for the ROM of the L-tab equipped blade section.

segment is referred to as Vortical structures Equivalent Trim Tab (VETT). These two latter segments can be in fixed position or follow a harmonic motion law, as well.

For oscillating motions of the tab and of the airfoil, multi-harmonic aerodynamic loads are observed, hence the system behaves non-linearly, consistently with experimental and numerical results reported in literature for similar devices, see e.g. Refs. [25, 48]. Nevertheless, the present aim is the identification of the aerodynamic response at the same frequency of the flap motion, since this is the main concern when vibration reduction algorithms, such as the HHC employed in the following, are considered on rotor blades. The linear ROM is indeed meant to reproduce the first harmonic component of the aerodynamic loads. The identification procedure is applied for several rotations of the L-tab in the steady case. For harmonic motions the identification is carried out separately for various reduced frequencies. The ROM is derived trying to minimize the error between the CFD-computed lift and moment coefficients [37] (the first harmonic component for unsteady motions) and the corresponding quantities resulting from the KS theory applied on the geometry shown in fig. 3.

A very good agreement between the loads numerically computed with CFD simulations and those resulting from the ROM is obtained both for steady state and oscillating motions of the airfoil and of the L-tab. For the steady state configuration the predictive capabilities of the model are also demonstrated [37, 45].

Among the three DOFs of the blade section model the harmonic motion of the L-tab appears to be the most challenging to be correctly reproduced. An example of the high quality fitting that is obtained for this motion is reported in fig. 4, where the first harmonic of the CFD computed lift and moment curve versus  $\beta$  is represented, together with the corresponding hysteresis loops resulting from the ROM at  $k = 0.1$  and  $k = 0.6$ , respectively. The identification procedure is carried out at several reduced frequencies of the tab motion separately. This allows to investigate the sensitivity of the ROM parameters to this input quantity. Figure 5 reports the free parameters achieved after the optimization procedure, versus the corresponding reduced frequency, which ranges from  $k = 0.1$  to  $k = 0.6$ . In particular in figure 5(a) the length of the VETT is rescaled with respect to the unitary chord of the numerical geometry. Hence the shift of  $\chi_w = \chi_w(x_c)$  with respect to the unity, directly quantifies the effect of chord enlargement induced by the L-tab. Notice that no significant excursions of the parameters with respect to  $k$  are encountered. Moreover the quite regular and smooth shape of the curves reported in fig. 5 allows to approximate such quantities with a low order polynomial. Therefore with the present ROM it appears possible to easily compute the mean line shape and the aerodynamic loads for arbitrary values of  $k$  in the range [0.1 0.6].

### 3. COMPARISON BETWEEN THE L-TAB AND A CLASSICAL TRAILING EDGE FLAP BY MEANS OF THIN LINE MODELS

Modifications in the effective camber equivalent to those induced by the L-tab could be obtained with a classical trailing edge flap. Nevertheless, whereas the same shape of the mean line can be potentially achieved both with the present L-tab, and with a classical trailing edge flap, the loads generated by the two configurations are expected to be different. Indeed the CRV past the L-tab do not directly contribute to the generation of the aerodynamic loads, that is such vortical structures do not act as a lifting surface, not being a solid body. Rather the CRV modify the pressure distribution along the airfoil, ultimately affecting the resulting aerodynamic loads. On the other hand, a classical trailing edge flap behaves indeed as a lifting surface, capable to develop aerodynamic loads by itself. Of course, also the upstream effect in the pressure distribution is expected to be different,

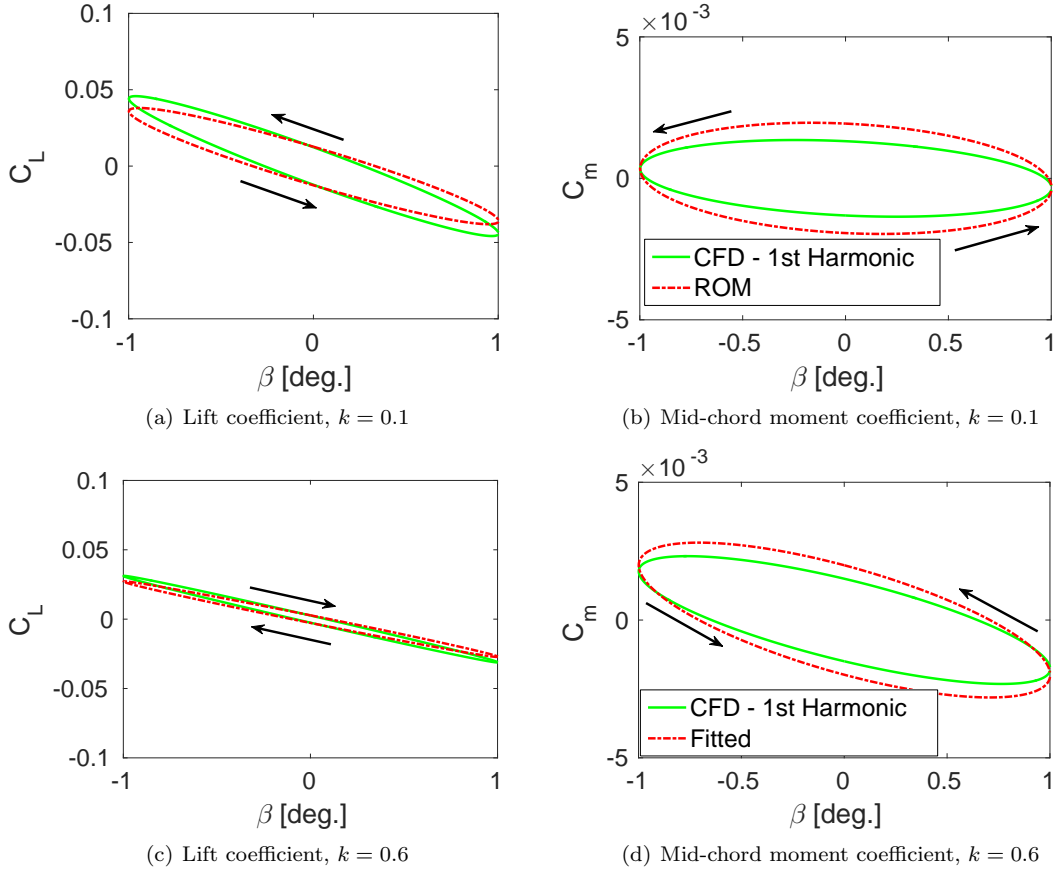


Figure 4: Comparison between the numerical 1st harmonic component of aerodynamic loads and their counterpart from the KS-based ROM at  $k = 0.1$  and  $k = 0.6$ ;  $\beta = 1 + 1 \sin(\omega t)$  deg.,  $\alpha = 0$  deg.,  $M = 0.117$ ,  $\text{Re} = 1 \cdot 10^6$ . The directions of the hysteresis loops are also reported.

when dealing with a trailing edge flap, rather than with a Gurney flap like device.

It appears interesting to gain an overview on the behavior of the aerodynamic loads potentially generated by these two different trailing edge configurations. This allows to preliminary estimate which solution, among the present L-tab and a classical flap, is more suitable to reduce vibratory loads at different frequencies. With this regard Friedmann [33] and Palacios [34] already compared the aerodynamic performance of GF like devices to those of trailing edge micro-flaps [33] and plain flaps [34]. They both found the behavior of the two trailing edge solutions comparable and, for some aspects, GF like devices were found more suitable for rotorcraft applications. These results, obtained with accurate CFD computations [33, 34] and with experimental measurements [34] are an useful starting point for the comparison discussed in this section. Indeed a similar behavior has to be expected also in terms of the L-tab with respect to the trailing

edge flap.

Thin-line analytical low order models, as the one reported in section 2., are appropriate for this comparison, since these allow for a rapid and straightforward computation of the aerodynamic loads, given the reference geometry and the motion law. Figure 6 shows a schematic comparison between the two movable devices under consideration and the corresponding thin-line geometry. Notice that the flap is thought to take into account also the chord extension associated to the CRV past the L-tab. Therefore the second segment in the equivalent geometry of the flapped section has length equal to that of the ELT plus the VETT, as shown in fig. 6. The hinge of the flap has the same location of that of the L-tab. The values of  $\beta_f$  and  $\theta_c$ , computed with the identification procedures performed on the L-tab, are used for the model of the trailing edge flap, as well. Of course this latter configuration does not present the DOF related to  $\beta_w$ , i.e. the additional motion of the VETT with

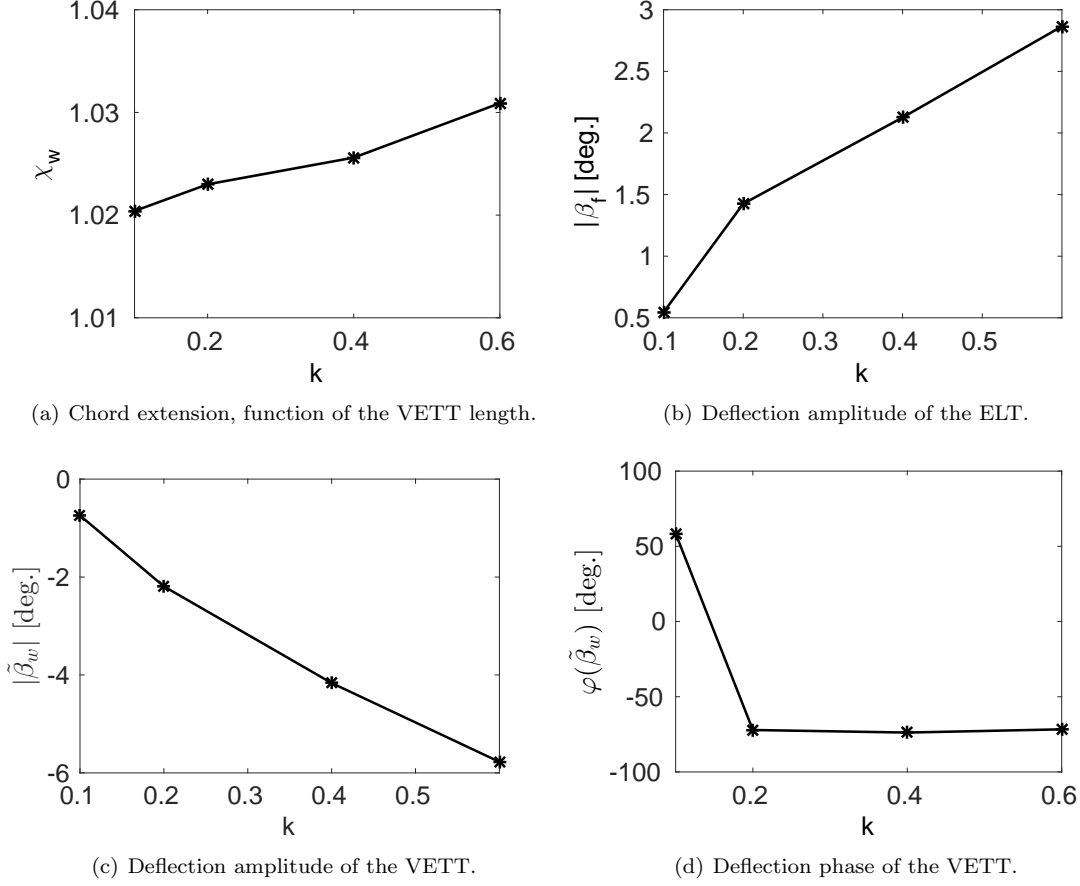


Figure 5: Values of the free parameters achieved after the optimization procedure at several reduced frequencies. The first parameter represents the effect of chord augmentation due to the CRV;  $\beta = 1 + 1 \sin(\omega t)$  deg.,  $\alpha = 0$  deg.,  $M = 0.117$ ,  $Re = 1 \cdot 10^6$ .

respect to the ELT.

It appears useful to remark that the second segment for the trailing edge flap model is meant to be entirely a solid body. Therefore, whereas for the L-tab model the pressure distribution is integrated from the leading edge (LE) up to  $x_c$ , for the trailing edge flap the integration domain ranges from the LE up to the trailing edge TE, see again figure 6. Once the resultants of the pressure distribution for the two configurations are computed, the aerodynamic loads have to be properly rescaled on the same chord length, to make them consistent and therefore comparable. Indeed the chord for the L-tab force coefficients ranges from  $x = \cos \pi = -1$  to  $x_c = \cos \theta_c < 1$ , being the total length  $(1 + \cos \theta_c)b < 2b$ , with  $b$  the semi-chord of the airfoil. On the other hand, the chord used to compute the airloads generated by the trailing edge flap ranges from  $x = \cos \pi = -1$  to  $x = \cos 0 = 1$ , being 2 the total length. Therefore the scaling fac-

tor between the lift coefficient of the trailing edge flap model  $C_{L_{\text{flap}}}$  and that of the L-tab model  $C_{L_{\text{tab}}}$  reads:

$$(1) \quad \frac{C_{L_{\text{flap}}}}{C_{L_{\text{tab}}}} = \frac{1 + x_c}{2}$$

For the pitching moment coefficient the scaling factor is computed as the square of the right hand side of eqn. (1). Figure 7 reports the magnitude and the phase of the properly scaled airloads, computed with the thin models for the L-tab and for the trailing edge flap, at several values of  $k$ . The force coefficients are also computed for fixed positions of the tab, i.e  $k = 0$ , namely at  $\beta = 1$  degree, which is the mean angle of oscillation for the unsteady motions herein taken into account. To this specific aim the steady state ROM mentioned in section 2. and discussed in detail in Refs. [37,45] is used. The parameters of the model for the steady

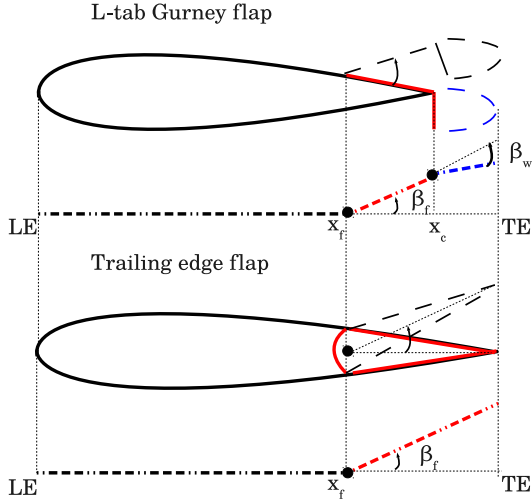


Figure 6: Thin line geometry for the ROMs; L-tab Gurney flap with the CRV (top) and classical plain trailing edge flap (bottom).

trailing edge flap are selected consistently with the approach adopted for the unsteady model. Figure 7(a) reports the magnitude of the lift coefficient versus the reduced frequency, including  $k = 0$ , obtained with the KS based models for the two trailing edge configurations. The L-tab grants larger lift in the range  $0.05 \leq k \leq 0.125$ ; the trailing edge flap seems to provide higher values of normal force for  $k < 0.05$  and for  $0.125 < k < 0.6$ . A slightly larger value of lift is achieved with the trailing edge flap for  $k = 0$  as well. Figure 7(c) shows the magnitude of the mid-chord moment coefficient for the L-tab and the flap models. Notice that for  $k > 0.0125$  the moment magnitude obtained with the L-tab is significantly larger with respect to the trailing edge flap. At  $k = 0.0125$  the two trailing edge configurations seem to provide the same pitching moment. A larger pitching moment is obtained at  $k = 0$  with the trailing edge flap.

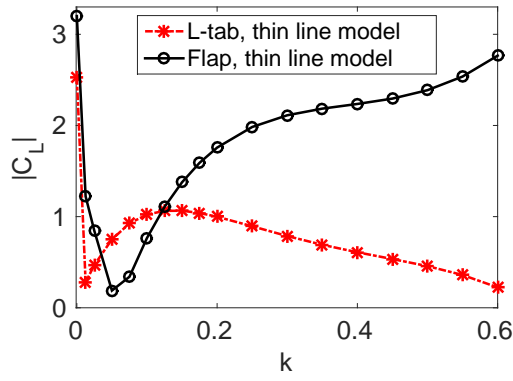
It appears also interesting to look at the loads distribution along the chord and again to compare the trailing edge configurations herein investigated.

Figure 8 reports the magnitude of the pressure distribution for the L-tab and the flap models at  $k = 0.1$  and  $k = 0.6$ . In particular figure 8(a) clearly shows that the area subtended by the red curve, related to the L-tab model, is larger than that covered by the black line, associated to the trailing edge flap. Figure 7(a) reports the magnitude of the lift coefficient versus the reduced frequency, including  $k = 0$ , attained with the cor-

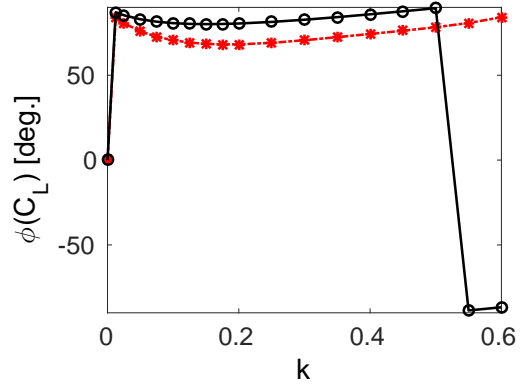
responding KS based models, for the two trailing edge configurations. Notice that, whereas the L-tab grants larger lift in the range  $0.05 \leq k \leq 0.125$ , the trailing edge flap seems to provide higher values of normal force for  $k < 0.05$  and for  $0.125 < k < 0.6$ . A slightly larger value of lift seems to be achieved with the trailing edge flap for  $k = 0$  as well. Figure 7(b) highlights that no significant differences are encountered in the phase of the lift coefficient for the two configurations at  $k < 0.5$ . Within this range the phase keeps almost constant with  $k$  and close to 90 degrees. At  $k \geq 0.5$  the lift phase of the flapped section changes in sign, assuming values near to -90 degrees. The lift coefficient phase is of course zero at  $k = 0$ . Figure 7(c) reports the magnitude of the mid-chord moment coefficient for the L-tab and the flap models. Notice that for  $k > 0.0125$  the moment magnitude attained with the L-tab is significantly larger with respect to the trailing edge flap. At  $k = 0.0125$  the two trailing edge configurations seem to provide the same pitching moment. A larger pitching moment is attained at  $k = 0$  with the trailing edge flap. The phase of the moment coefficient, reported in figure 7(d), is found to lie in the range [-90 90] degrees. At  $k \geq 0.125$  the pitching moment phase is larger for the L-tab. The opposite occurs at  $0 < k < 0.125$ , whereas, again, the pitching moment phase is equal to zero at  $k = 0$ . At  $k = 0.0125$  the pitching moment phase presents a local minimum for the L-tab and a local maximum for the trailing edge flap. In general the curve of the pitching moment phase related to the L-tab appears to be almost symmetrical to that of the trailing edge flap with respect to the  $\varphi(C_m) \approx 10$  deg. horizontal axis.

For completeness the lift coefficient hysteresis curves for the L-tab and the flap models at  $k = 0.1$  and  $k = 0.6$  are reported in figure 9. The behavior exhibited by the magnitude again confirms the results obtained in terms of the pressure distribution. Moreover it is shown that also the ROM for the trailing edge flap gives reasonable results if compared, for example, to the computations performed by Liu [33] on a similar trailing edge movable device, or to the analytical and numerical results reported in the textbook of Leishman [49], pp. 500-502.

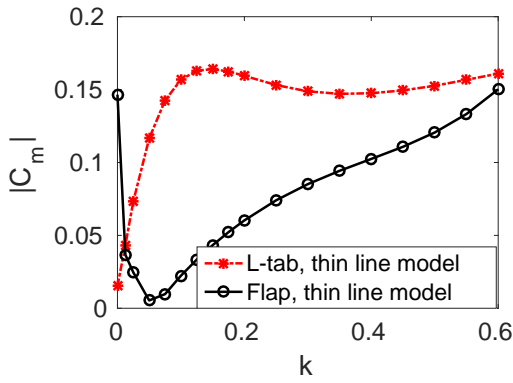
With regard to the magnitude of the loads, the trailing edge flap solution is found to develop larger normal forces on a wider range of frequencies, compared to the L-tab. On the other hand the L-tab provides larger values of the pitching moment at each of the reduced frequencies taken



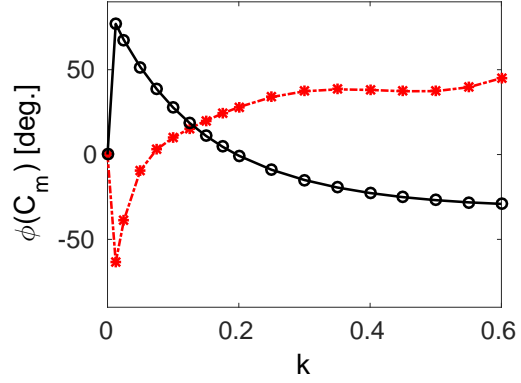
(a) Lift coefficient, magnitude.



(b) Lift coefficient, phase.

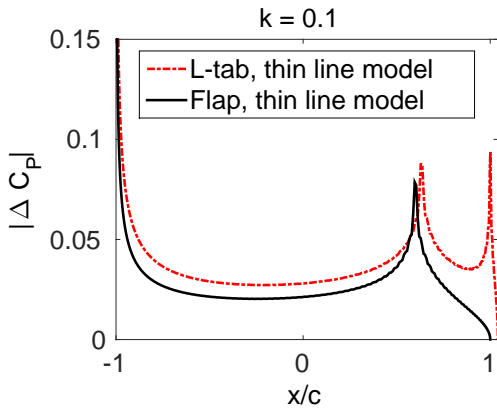


(c) Mid-chord moment coefficient, magnitude.

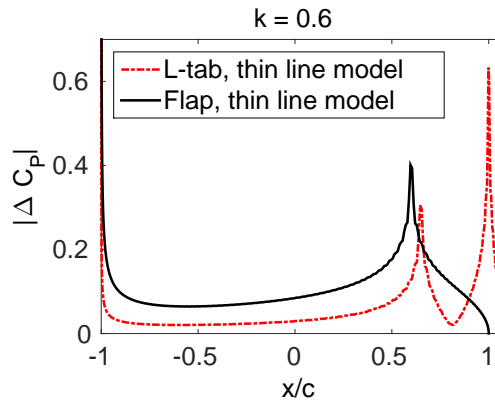


(d) Mid-chord moment coefficient, phase.

Figure 7: Magnitude and phase of the lift and pitching moment coefficients vs. the reduced frequency. Comparison between the L-tab and the flap models at  $\beta = 1$  deg. and  $\beta = 1 + \sin(\omega t)$  degrees;  $M = 0.117$ ,  $Re = 1 \cdot 10^6$ .



(a)  $k = 0.1$



(b)  $k = 0.6$

Figure 8: Pressure coefficient magnitude along the chord of the model. Comparison between the L-tab and the trailing edge flap models at  $k = 0.1$  and  $k = 0.6$ ;  $\beta = 1 + \sin(\omega t)$  degrees,  $M = 0.117$ ,  $Re = 1 \cdot 10^6$ .

under consideration, but at  $k < 0.0125$ .

The ultimate selection of the control surface to be employed is somehow tricky, since several as-

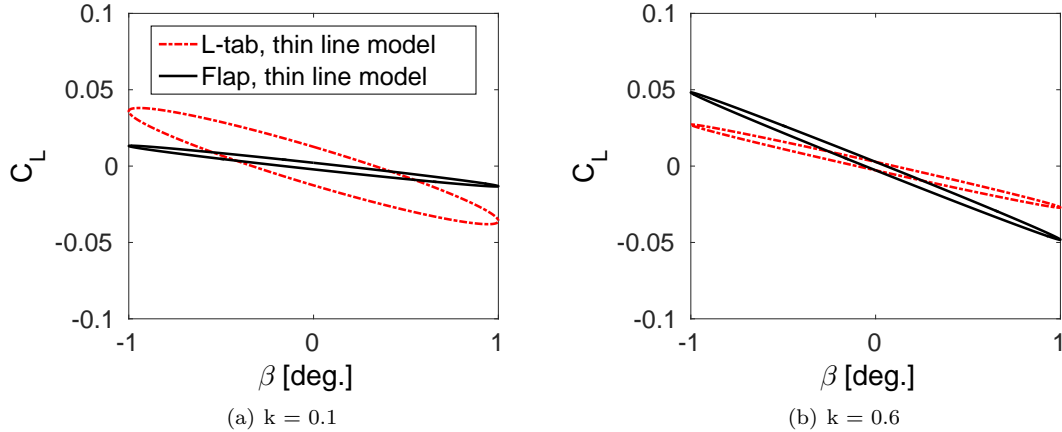


Figure 9: Lift coefficient hysteresis curves. Comparison between the L-tab and the trailing edge flap models at  $k = 0.1$  and  $k = 0.6$ ;  $\beta = 1 + \sin(\omega t)$  degrees,  $M = 0.117$ ,  $Re = 1 \cdot 10^6$ .

pects have to be taken together under consideration. Of course the choice can not be based merely on the magnitude of lift and moment coefficients developed for steady state configurations or small amplitude oscillations, but it must take into account also technological aspects. The preliminary comparison reported in this work has the primary aim of showing that both the steady and the unsteady airloads developed by the present L-tab are similar to those generated by a classical trailing edge flap configuration, widely diffused in literature, at least up to  $k = 0.15$ . The capabilities of vibration reduction of both these devices will be investigated in the following. It appears useful to recall that, among the additional operations of such movable devices on rotor blades, the performance enhancement and the dynamic stall alleviation are of primary interest. In this context acting on the pitching moment appears to be more effective, rather than on the lift, since by acting directly on the blade twist, the angle of attack can be locally controlled and properly set to the values required, e.g. for static load balance or to avoid the stall onset. Furthermore considerations concerning actuation and stowage requirements, as those reported in the work of Palacios [34], affect the ultimate choice of the trailing edge device for the rotor blade. With this regard the employment of the L-tab appears to be very promising since its small weight features should allow for lower power and in turn smaller and lighter actuation systems, with respect to those required for classical trailing edge flaps.

#### 4. AEROELASTIC MODEL FOR THE BLADE SECTION WITH THE L-TAB

An analytical formulation based on the typical section model [50] is used to investigate the aeroelastic response of the blade section equipped either with the L-tab or with a classical flap. Details of this largely employed approach can be found for instance in the textbook of Johnson [51], chapter 16. The aerostructural model has three DOFs, namely pitch and plunge oscillations of the airfoil, in addition to the rotation of the control  $\beta_{\text{cont}}$ , positive upward. According to classical approaches adopted to model the blade dynamics [51], the plunge motion is written as a function of the local bending, namely  $h = -\beta_{\text{bl}} r$ , being  $\beta_{\text{bl}}$  the flapping angle and  $r$  the local radius on the blade. Consistently with the classical notation, the pitch of the blade is referred to as  $\theta$ . The resulting 3x1 complex array of the blade DOFs is therefore  $\mathbf{q} = [\beta_{\text{bl}} \ \theta \ \beta_{\text{cont}}]^T$ .

The aeroelastic model is sketched in fig. 10. The bending stiffness is represented by a translational spring of non-dimensional stiffness  $\nu_{\beta}$ , equivalent to the rotating natural frequency of flap mode for the blade model. On the other hand the torsional stiffness, is represented by means of a torsional spring of non-dimensional stiffness  $\nu_{\theta}$ , equivalent to the rotating natural frequency of the torsion mode for the blade model. The trailing edge movable device has non-dimensional torsional stiffness  $\nu_{\beta f}$ . The blade mass is referred to as  $M_{\text{bl}}$ , whereas its flap and feathering moments of inertia are referred to as  $I_b$  and  $I_f$ , respectively. The bending static moment of the blade is referred to as  $I_s$ . To



$$(4) \quad \bar{M}_{\beta_{bl}} = \frac{1}{\rho 2\pi c \Omega^2 R^4} \int_0^R r L dr$$

$$(5) \quad \bar{M}_\theta = \frac{1}{\rho 2\pi c \Omega^2 R^4} \int_0^R M_{c/4} dr$$

$$(6) \quad \bar{M}_{h_{\beta_{cont}}} = \frac{1}{\rho 2\pi c \Omega^2 R^4} \int_0^R M_h dr,$$

where  $R$  is the blade radius and  $\rho$  is the freestream density. Notice that no offset is herein assumed for the aerodynamic center with respect to the elastic axis, which is coincident with the feathering axis. Therefore the resulting aerodynamic system can be written in non-dimensional form as:

$$(7) \quad \begin{bmatrix} \bar{M}_{\beta_{bl}} \\ \bar{M}_\theta \\ \bar{M}_{h_{\beta_{cont}}} \end{bmatrix} \begin{bmatrix} \beta_{bl} \\ \theta \\ \beta_{cont} \end{bmatrix} = \mathbf{H}_{am} \mathbf{q} = \\ = \begin{bmatrix} h_{\beta_{bl}\beta_{bl}} & h_{\beta_{bl}\theta} & h_{\beta_{bl}\beta_{cont}} \\ h_{\theta\beta_{bl}} & h_{\theta\theta} & h_{\theta\beta_{cont}} \\ h_{\beta_{cont}\beta_{bl}} & h_{\beta_{cont}\theta} & h_{\beta_{cont}\beta_{cont}} \end{bmatrix}$$

The symmetrical mass matrix is [51]:

$$(8) \quad \mathbf{M} = \frac{1}{\Omega^2} \begin{bmatrix} 1 & -\frac{3}{2} \frac{x_I}{R} & 0 \\ -\frac{3}{2} \frac{x_I}{R} & \bar{I}_f & 0 \\ 0 & 0 & 0 \end{bmatrix},$$

where  $x_I$  is the offset of the blade center of gravity with respect to its feathering axis (negative upstream the feathering axis) and  $\bar{I}_f$  is the ratio between the feather moment of inertia  $I_f$  and the flap moment of inertia  $I_b$ .

The symmetrical stiffness matrix, also made dimensionless with respect to the blade flap moment of inertia, is [51]:

$$(9) \quad \mathbf{K} = \begin{bmatrix} \nu_\beta^2 & -\frac{3}{2} \frac{x_I}{R} & 0 \\ -\frac{3}{2} \frac{x_I}{R} & \bar{I}_f \nu_\theta^2 & 0 \\ 0 & 0 & 0 \end{bmatrix},$$

recalling that  $\nu_\beta$  is the rotating natural frequency of the flap mode and  $\nu_\theta$  is the rotating natural frequency of the pitch mode, both expressed in /rev.

Since  $\beta_{cont}$  is actually a control input, the aeroelastic transfer matrix  $\mathbf{Z}(j\omega)$  of eqn. (2) is split as follows:

$$(10) \quad \mathbf{Z}(j\omega) = \begin{bmatrix} \mathbf{Z}_{\beta_{bl}\theta} & \mathbf{Z}_{(\beta_{bl}\theta)\beta_{cont}} \\ \mathbf{Z}_{\beta_{cont}(\beta_{bl}\theta)} & \mathbf{Z}_{\beta_{cont}\beta_{cont}} \end{bmatrix}$$

This leads to:

$$(11) \quad \mathbf{Z}_{\beta_{cont}(\beta_{bl}\theta)} \begin{bmatrix} \beta_{bl} \\ \theta \end{bmatrix} = -\mathbf{Z}_{(\beta_{bl}\theta)\beta_{cont}} \beta_{cont}$$

$$(12) \quad \mathbf{Z}_{\beta_{bl}\theta} \begin{bmatrix} \beta_{bl} \\ \theta \end{bmatrix} + \mathbf{Z}_{\beta_{cont}\beta_{cont}} \beta_{cont} = \bar{M}_{h_{\beta_{cont}}}$$

Eqn. (12) can be used to check the suitability of the control input, computed by means of eqn. (11), with respect to the operating capabilities of the actuation system. The system response array  $[\beta_{bl} \theta]^T$  may be then expressed as:

$$(13) \quad \begin{bmatrix} \beta_{bl} \\ \theta \end{bmatrix} = \begin{bmatrix} \beta_{bl_0} \\ \theta_0 \end{bmatrix} + \begin{bmatrix} \beta_{bl} \\ \theta \end{bmatrix} = \mathbf{z}_0 + \mathbf{z},$$

being  $\mathbf{z}_0$  the uncontrolled response and  $\mathbf{z}$  the system response to the control input [42, 53].

Accordingly, eqn. (11) is written as:

$$(14) \quad \mathbf{Z}_{\beta_{bl}\theta} \begin{bmatrix} \beta_{bl} \\ \theta \end{bmatrix} = -\mathbf{Z}_{\beta_{bl}\theta} \begin{bmatrix} \beta_{bl_0} \\ \theta_0 \end{bmatrix} - \mathbf{Z}_{(\beta_{bl}\theta)\beta_{cont}} \beta_{cont}$$

For further convenience the matrices of eqn. (14) may be renamed as follows:

$$(15) \quad \mathbf{X} \mathbf{z} = -\mathbf{X} \mathbf{z}_0 - \mathbf{F} \beta_{cont}$$

On the right hand side in eqn. (15) the first term represents the forcing of the system, whereas the second term is the input control force. The state variables of the aerostructural system, i.e. the system response, can ultimately be expressed as:

$$(16) \quad \mathbf{z} = -\mathbf{z}_0 - \mathbf{X}^{-1} \mathbf{F} \beta_{cont}$$

According to the classical notation employed for the HHC formulations [16, 42, 53], eqn. (16) can be written as

$$(17) \quad \mathbf{z} = -\mathbf{z}_0 - \mathbf{T} \beta_{cont},$$

where  $\mathbf{T} = \mathbf{X}^{-1} \mathbf{F}$ . As a result the control force  $\bar{\mathbf{F}}_c^{2 \times 1}$  in terms of flap and pitch moments at the blade root, developed by the trailing edge device, reads

$$(18) \quad \bar{\mathbf{F}}_c = -\mathbf{X}^{-1} \mathbf{F} \beta_{cont}$$

Consistently, the flap and pitch moment at the blade root for the uncontrolled system can be written as

$$(19) \quad \bar{\mathbf{F}}_{uc} = -\mathbf{X}^{-1} \mathbf{z}_0$$

Among the load components which most affect the vibration transmitted from the blades to the rotor hub there is the vertical force  $F_z$ . This quantity is expressed as the output equation of the aeroelastic system described by the state eqn. (15). The aerodynamic vertical force on the blade is computed by assuming the lift as almost parallel to the  $z$  axis. The lift computed for each of the blade

sections, by taking into account the local speed and reduced frequency, is integrated to obtain the blade root non dimensional vertical aerodynamic force:

$$(20) \quad \bar{F}_{z_a} = \frac{1}{\rho\pi R^4 \Omega^2} \left( -[F_{z\beta_{bl}} \quad F_{z\theta}] \mathbf{z} + F_{z\beta_{cont}} \beta_{cont} \right)$$

$F_{z\beta_{bl}}$  gives the vertical force for a unitary bending rotation of the blade,  $F_{z\theta}$  provides the vertical force for a unitary pitch rotation of the blade, whereas  $F_{z\beta_{cont}}$  determines the vertical force for a unitary rotation of the control surface. Notice that the first term of the right hand side in eqn. (20) is opposite in sign with respect to the second term. As an example, by imposing a downward rotation to the control surface, the blade undergoes an upward flapping motion, which in turn leads to negative aerodynamic forces generated by plunge and pitch oscillations. That is the aerodynamic vertical force related to flapping and pitching motions of the blade is opposite in sign with respect to the vertical force generated by deflecting the control surface. The final expression for the non dimensional vertical force  $\bar{F}_z$  at the blade root includes the blade bending inertial force. Therefore

$$(21) \quad \bar{F}_z = \frac{1}{\rho\pi R^4 \Omega^2} \left( -[F_{z\beta_{bl}} \quad F_{z\theta}] \mathbf{z} + F_{z\beta_{cont}} \beta_{cont} - \Omega^2 I_s \beta_{bl} \right), \quad (25)$$

where the bending inertial force  $\Omega^2 I_s \beta_{bl}$  is again opposite in sign with respect to the blade flapping induced by the rotation of the control surface.

## 5. HIGHER HARMONIC CONTROL FOR THE BLADE VIBRATION REDUCTION

The HHC approach [16,42,53] is employed to compute the potential vibration reduction capabilities of the L-tab, compared to those provided by the trailing edge flap described in section 3.. According to Johnson [42] three primary features characterize HHC algorithms: a linear, quasi-static frequency domain model of the helicopter response; an identification procedure carried out by means of a least squares or a Kalman filter method; the employment of a quadratic-form figure of merit. The HHC algorithm herein proposed presents indeed all of these properties.

Since the HHC approach is conceived to minimize vibratory loads for one specific frequency at time [16], proper control inputs are computed separately for the 2/rev, 3/rev, 4/rev and 5/rev loads. A figure of merit  $J$  including the blade root flap and pitch moments, in addition to the vertical shear, is employed for computing the optimal

control input  $\beta_{cont}$  to be applied. Namely the functional contains the 3x1 array  $\mathbf{L} = [\bar{M}_{\beta_{bl}} \quad \bar{M}_\theta \quad \bar{F}_z]^T$ :

$$(22) \quad J = \begin{bmatrix} \bar{M}_{\beta_{bl}} \\ \bar{M}_\theta \\ \bar{F}_z \end{bmatrix}^T [\mathbf{W}] \begin{bmatrix} \bar{M}_{\beta_{bl}} \\ \bar{M}_\theta \\ \bar{F}_z \end{bmatrix} + \beta_{cont}^T R_{cont}^{1 \times 1} \beta_{cont}$$

where the transpose operation involves also the computation of the complex conjugate. Accordingly  $\beta_{cont}^T$  is the complex conjugate of  $\beta_{cont}$ . The diagonal matrix  $\mathbf{W}$  specifies the weights for the controlled variables, whereas the scalar  $R_{cont}$  weights the control input authority. The array of the loads in eqn. (22) has to be expressed as a function of the control input  $\beta_{cont}$ . For convenience the following matrices are introduced:

$$(23) \quad \tilde{\mathbf{F}}_z = \frac{1}{\rho\pi R^4 \Omega^2} \left( [F_{z\beta_{bl}} \quad F_{z\theta}] + [\Omega^2 I_s \quad 0] \right)$$

$$(24) \quad \mathbf{B} = \begin{bmatrix} \mathbf{0} \\ \tilde{\mathbf{F}}_z \end{bmatrix}$$

$$\mathbf{C} = \begin{bmatrix} -\mathbf{F} \\ F_{z\beta_{cont}} \end{bmatrix},$$

where the matrix  $\mathbf{F}$  is the one that appears in eqn. (15). The following matrices are also introduced, to conveniently express  $J$ .

$$(26) \quad \mathbf{L}_0 = \begin{bmatrix} \mathbf{F}_{uc} \\ 0 \end{bmatrix} - \mathbf{B} \mathbf{z}_0,$$

$$(27) \quad \mathbf{L}_{cont} = -\mathbf{B}\mathbf{X}^{-1}\mathbf{F} + \mathbf{C},$$

where the array of the uncontrolled flap and pitch moments  $\mathbf{F}_{uc}$  is the one introduced in eqn. (19). The 3x1 array  $\mathbf{L}$ , containing the loads to be minimized, can now be written as a function of  $\beta_{cont}$  as follows:

$$(28) \quad \mathbf{L} = \mathbf{L}_0 + \mathbf{L}_{cont} \beta_{cont}$$

As a result the figure of merit of eqn. (22) reads:

$$(29) \quad J = \left( \mathbf{L}_0^T + \beta_{cont}^T \mathbf{L}_{cont}^T \right) \mathbf{W} \left( \mathbf{L}_0 + \mathbf{L}_{cont} \beta_{cont} \right) + \beta_{cont}^T R_{cont} \beta_{cont}$$

By imposing  $dJ/d\beta_{cont} = 0$  the control input can be computed as follows:

$$(30) \quad \beta_{cont} = - \left( \mathbf{L}_{cont}^T \mathbf{W} \mathbf{L}_{cont} + R_{cont} \right)^{-1} \left( \mathbf{L}_0^T \mathbf{W} \mathbf{L}_0 \right).$$

Table 1: Geometrical, inertial and elastic main properties of the blade for a Bo-105 rotor model.

Parameters	Values
blade radius, $R$	4.9000 m
blade mass, $M_{bl}$	50.6061 kg
blade flap moment of inertia, $I_b$	209.9097 kg m <sup>2</sup>
blade feathering moment of inertia, $I_f$	0.1059 kg m <sup>2</sup>
rotor angular velocity, $\Omega$	44.4010 rad/s
rotating natural frequency of the blade flap mode, $\nu_\beta$	1.1080 /rev
rotating natural frequency of the blade torsion mode, $\nu_\theta$	3.8210 /rev
Lock number, $\gamma$	5.5
blade chord, $c$	0.27 m
Elastic Axis, EA	0
feathering axis	0 $\equiv$ EA
aerodynamic center	0 $\equiv$ EA
Center of Gravity, CG	-0.5439 m
Hinge Axis, HA	0.8c
x axis origin	$c/4 \equiv$ EA
helicopter advance ratio, $\mu$	0.2

A blade model for a hingeless Bo-105 rotor is herein used as test application for the present control system. The values of the blade model properties, used to evaluate the matrices of the aeroelastic system, are reported in table 1.

Figure 12 reports the vibratory blade root loads in the rotating frame corresponding to the baseline and controlled configurations—with both the L-tab and the TE flap models—for the 2/rev and 3/rev harmonic components. The values of the control input magnitude and phase, obtained by minimizing the figure of merit in eqn. (29), are also reported. Both the L-tab and the TE flap is found to break down almost the 100% of the vertical force and of the bending moment. On the other hand, the root pitching moment appears substantially unaffected by the movable device. The optimal control input of the L-tab is slightly smaller than that of the TE flap. Notice that such values of the control inputs are not dissimilar to those obtained by Chopra [18, 54], with analogous trailing edge solutions. The phase angle of the control input at 2/rev and 3/rev lies in the range [-125 -75] degrees, for both the L-tab and the TE flap.

Figure 13 shows the vibratory rotating frame blade root loads corresponding to the baseline and to the configuration with the L-tab and TE flap models, for the 4/rev and 5/rev harmonic components. The control input magnitude and phase, obtained by minimizing the figure of merit of eqn. (29), are also reported. The blade root flapping moments are almost completely canceled,

whereas the vertical forces undergo reductions superior to 90%. Similarly to what observed for the 2/rev and 3/rev harmonics, no significant effects of the control devices on the blade root pitching moment can be obtained. The optimal control input amplitude obtained for the L-tab is slightly larger with respect to that of the TE flap. The input control amplitude is again not dissimilar to the values computed by Chopra [18, 54] on a TE flap employed for rotorcraft vibration reductions. The phase angle of the control inputs is positive for the 4/rev harmonic and negative for the 5/rev component.

As expected, both the L-tab and the TE flap are found not capable to alleviate the blade root pitching moment. This is due to the large torsional stiffness, typical of most rotor blades. The local flapping caused by the rotation of the movable device propagates along the entire span, providing a significant magnification factor to the action of the control surface, this does not occur for the blade torsion. To obtain a more effective action on the blade twist, which in turn is transmitted to the main rotor through the pitch links, a distribution of several L-tabs or TE flaps along the span should be employed, see for instance the work of Lemmens [55]. Alternatively a new blade, with a significantly smaller torsional stiffness, should be conceived, to allow for the propagation of the local blade torsion, induced by the control surface, along the entire span.

Table 2 reports the values of the reference reduced frequency, computed at the 75% of the blade

span as  $k = \omega b / \Omega 0.75R$ , being  $\omega$  the /rev frequency, ranging from 2/rev to 5/rev. In this way it is possible to immediately relate the results discussed in this section with those reported in figs. 7(a), 8(a) and 9. Notice that for 2/rev and 3/rev  $k < 0.125$ . Therefore, according to fig. 7(a) the L-tab provides larger values of lift, for equal rotations of the movable device. This is consistent with the results reported in fig. 12, in terms of the computed control input amplitude. Indeed, to achieve almost the same control force –and in turn load alleviation– the TE flap requires a larger rotation amplitude with respect to the L-tab. On the other hand, for 4/rev and 5/rev the corresponding reference  $k$  is greater than 0.125. Consistently, almost analogous reductions in the vertical force and in the bending moment are obtained with slightly larger rotations of the L-tab with respect to the flap. The magnitude of the computed control inputs for the L-tab and the TE flap models at N/rev are reported versus the related harmonics in fig. 14. These last remarks give further confirmation to what observed by simply considering the aerodynamic forces developed by the two TE devices, see section 3.. That is, by coupling the aerodynamic models to the blade dynamics, no unexpected or undesired effects are encountered.

Parameters	Values			
harmonics	2/rev	3/rev	4/rev	5/rev
$k$	0.0735	0.1102	0.1469	0.1837

Table 2: Reduced frequency, evaluated at 0.75R, corresponding to considered the harmonics of the loads and of the control inputs.

## 6. CONCLUSIONS

The capabilities of a novel L-shaped Gurney flap in alleviating vibration on helicopter blades are investigated. A physically based ROM is built for a blade section equipped with such L-tab, on the basis of numerical simulations previously validated with experimental results. Additionally the aerodynamic loads developed by a classical trailing edge flap, modeled again as a piece-wise mean line, are computed. Overall the L-tab and the TE flap provide not dissimilar values of lift and pitching moment, if one remains at  $k$  lower than 0.15, being such values indeed consistent with vibration reduction problems on helicopter blades.

Typical section aerostructural models are then built up for a helicopter blade equipped with ei-

ther the L-tab or the TE flap. The rotating frame blade root aerodynamic loads are computed by integrating along the span the airloads achieved with the developed physically based ROMs. An analytical formulation, is used to build the mass and the stiffness matrices of the blade. A Higher Harmonic Control approach is employed to compute a single-frequency control input, aiming to reduce the bending moment, the pitching moment and the vertical force at the blade root in terms of the 2/rev, 3/rev, 4/rev and 5/rev harmonics, respectively. It is found that both the L-tab and the TE flap are capable to alleviate almost the 100% of the vertical force and of the bending moment at N/rev. Consistently with the aerodynamic performance provided by the two movable devices at  $k < 0.125$ , the TE flap is found to require slightly larger amplitudes of the control inputs, with respect to the L-tab. With regard to the blade root pitching moment, no significant alleviations are obtained with the L-tab as well as with the TE flap, for each of the harmonics under consideration.

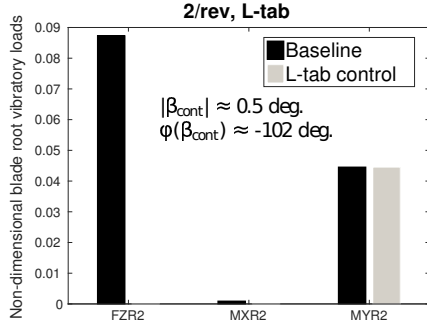
Overall the present concept of trailing edge L-shaped movable device is potentially suitable to be used as alternative vibration reduction system on rotor blades. Advantages with respect to the employment of classical plain flaps or movable GFs are expected in terms of power requirements and operation of actuation systems, respectively.

## References

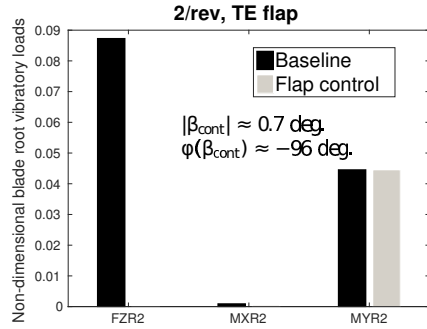
- [1] Katz, J., “Aerodynamics of Race Cars,” *Annual Review of Fluid Mechanics*, Vol. 38, No. 1, 2006, pp. 27–63.
- [2] Liebeck, R. H., “Design of Subsonic Airfoils for High Lift,” *Journal of Aircraft*, Vol. 15, No. 9, 1978, pp. 547–561.
- [3] Kentfield, J., “The potential of Gurney flaps for improving the aerodynamic performance of helicopter rotors,” *International Powered Lift Conference, Santa Clara, CA, USA*, American Institute of Aeronautics and Astronautics, Dec. 1993.
- [4] Storms, B. L. and Jang, C. S., “Lift Enhancement of an Airfoil Using a Gurney Flap and Vortex Generators,” *Journal of Aircraft*, Vol. 31, No. 3, May-Jun. 1994, pp. 542–547.
- [5] Myose, R. Y., Papadakis, M., and Heron, I., “Gurney Flap Experiments on Airfoils, Wings, and Reflection Plane Model,” *Journal of Aircraft*, Vol. 35, No. 2, Mar.-Apr. 1998, pp. 206–211.
- [6] Papadakis, M., Myose, R. Y., Heron, I., and Johnson, B. L., “An experimental investigation of Gurney flaps on a GA(W)-2 airfoil with 25% slotted

- flap,” *14th AIAA Applied Aerodynamic Conference, AIAA Paper 1996-2437*, 1996.
- [7] Zhang, W., Wang, J. J., and Wu, Z., “Experimental investigations on the application of lift enhancement devices to forward-swept aircraft model,” *The Aeronautical Journal*, Vol. 110, No. 1108, June 2006, pp. 361–367.
- [8] Wang, J. J., Li, Y. C., and Choi, K. S., “Gurney flap–Lift enhancement, mechanisms and applications,” *Progress in Aerospace Sciences*, Vol. 44, No. 1, Jan. 2008, pp. 22–47.
- [9] Baker, J. P., Standish, K. J., and van Dam, C. P., “Two-Dimensional Wind Tunnel and Computational Investigation of a Microtab Modified Airfoil,” *Journal of Aircraft*, Vol. 44, No. 2, Mar.-Apr. 2007, pp. 563–572.
- [10] Maughmer, M. and Bramesfeld, G., “Experimental Investigation of Gurney Flaps,” *Journal of Aircraft*, Vol. 45, No. 6, Nov.-Dec. 2008, pp. 2062–2067.
- [11] Giguère, P., Lemay, J., and Dumas, G., “Gurney Flap Effects and Scaling for Low-Speed Airfoils,” *AIAA Paper 95-1881-CP*, 1995.
- [12] Jang, C. S., Ross, J. C., and Cummings, R. M., “Numerical Investigation of an Airfoil with a Gurney Flap,” *Aircraft Design*, Vol. 1, No. 2, June 1998, pp. 75–88.
- [13] Jeffrey, D., Zhang, X., and Hurst, D., “Aerodynamics of Gurney Flaps on a Single-Element High-Lift Wing,” *Journal of Aircraft*, Vol. 37, No. 2, 2000, pp. 295–301.
- [14] Standish, K. J. and van Dam, C. P., “Computational Analysis of a Microtab-Based Aerodynamic Load Control System for Rotor Blades,” *AHS 4th Decennial Specialist’s Conference on Aeromechanics*, Jan. 2004.
- [15] Motta, V., Guardone, A., and Quaranta, G., “Numerical investigation of an L-shaped deployable Gurney flap for rotorcraft vibration control,” *International Forum on Aeroelasticity and Structural Dynamics, Bristol, UK*, 24–26 June 2013.
- [16] Friedmann, P. P. and Millott, T. A., “Vibration Reduction in Rotorcraft Using Active Control: A Comparison of Various Approaches,” *Journal of Guidance, Control, and Dynamics*, Vol. 18, No. 4, 1995, pp. 664–673.
- [17] Milgram, J., Chopra, I., and Straub, F., “Rotors With Trailing Edge Flaps: Analysis and Comparison With Experimental Data,” *Journal of the American Helicopter Society*, Vol. 43, No. 4, 1998, pp. 319–332.
- [18] Roget, B. and Chopra, I., “Control of Dissimilar Rotor Vibration,” *43rd AIAA/ASME/ASCE/AHS/ASC Structures, Structural Dynamics and Materials Conference, Denver, CO*, 22–25 April 2002.
- [19] Shen, J., Yang, M., and Chopra, I., “Swashplate-less Helicopter Rotor System with Active Trailing-Edge Flaps for Primary and Vibration Controls,” *45th AIAA/ASME/ASCE/AHS/ASC Structures, Structural Dynamics and Materials Conference, Palm Springs, CA*, 19–22 April 2004.
- [20] Roget, B. and Chopra, I., “Wind-Tunnel Testing of Rotor with Individually Controlled Trailing-Edge Flaps for Vibration Reduction,” *Journal of Aircraft*, Vol. 45, No. 3, 2008, pp. 868–879.
- [21] Greenblatt, D., Nishri, B., Darabi, A., and Wygnanski, I., “Dynamic Stall Control by Periodic Excitation, Part 2: Mechanisms,” *Journal of Aircraft*, Vol. 38, No. 3, May-Jun. 2001, pp. 439–447.
- [22] Feszty, D., Gillies, E. A., and Vezza, M., “Alleviation of Airfoil Dynamic Stall Moments via Trailing-Edge Flap Flow Control,” *AIAA Journal*, Vol. 42, No. 1, Jan. 2004, pp. 17–25.
- [23] Lee, H. and Su, Y. Y., “Unsteady airfoil with a harmonically deflected trailing-edge flap,” *Journal of Fluids and Structures*, Vol. 27, No. 27, 2011, pp. 1411–1424.
- [24] Lee, T. and Gerontakos, P., “Oscillating Wing Loadings with Trailing-Edge Strips,” *Journal of Aircraft*, Vol. 43, No. 2, Mar.-Apr. 2006, pp. 428–436.
- [25] Tang, D. and Dowell, E. H., “Aerodynamic Flow Control of an Airfoil with Small Trailing-Edge Strips,” *Journal of Aircraft*, Vol. 43, No. 6, Nov.-Dec. 2006, pp. 1854–1866.
- [26] Tang, D. and Dowell, E. H., “Aerodynamic Loading for an Airfoil with an Oscillating Gurney Flap,” *Journal of Aircraft*, Vol. 44, No. 4, Jul.-Aug. 2007, pp. 428–436.
- [27] Kinzel, M., Maughmer, M., and Duque, E., “Numerical Investigation on the Aerodynamics of Oscillating Airfoils with Deployable Gurney Flaps,” *AIAA Journal*, Vol. 48, No. 7, 2010, pp. 1457–1469.
- [28] Li, Y., J., W., and Zhang, P., “Influences of Mounting Angles and Locations on the Effects of Gurney Flaps,” *Journal of Aircraft*, Vol. 40, No. 3, May-Jun. 2003, pp. 494–498.
- [29] Cole, J. A., Vieira, B. A., Coder, J. G., Premi, A., and Maughmer, M. D., “Experimental Investigation into the Effect of Gurney Flaps on Various Airfoils,” *Journal of Aircraft*, Vol. 50, No. 4, Jul.-Aug. 2013, pp. 1287–1294.
- [30] Matalanis, C. G., Wake, B. E., Opoku, D., Min, B., Yeshala, N., and Sankar, L., “Aerodynamic Evaluation of Miniature Trailing-Edge Effectors for Active Rotor Control,” *Journal of Aircraft*, Vol. 48, No. 3, 2011, pp. 995–1004.
- [31] Min, B. Y., Sankar, L., and Bauchau, O. A., “A CFD-CSD Coupled-Analysis of HART-II Rotor

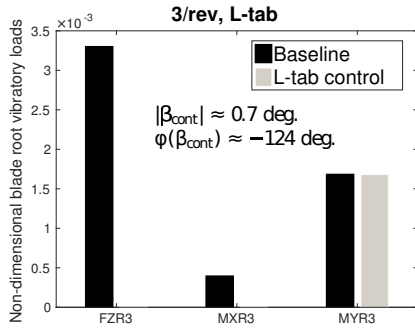
- Vibration Reduction using Gurney Flaps,” *Proceedings of the American Helicopter Society 66th Forum and Technology Display, Phoenix, AZ*, 2010.
- [32] Yu, Y. H., Tung, C., van der Wall, B. G., Pausder, H., Burley, C., Brooks, T., Beaumier, P., Delrieux, Y., Mercker, E., and Pengel, K., “The HART-II Test: Rotor Wakes and Aeroacoustics with Higher-Harmonic Pitch Control (HHC) Inputs – The Joint German/French/Dutch/US Project,” *American Helicopter Society 58th Annual Forum, Montreal, Canada*, 11–13 June 2002.
- [33] Liu, L., Padthe, A. K., and Friedmann, P. P., “Computational Study of Microflaps with Application to Vibration Reduction in Helicopter Rotors,” *AIAA Journal*, Vol. 49, No. 7, July 2011.
- [34] Palacios, J., Kinzel, M., and Overmeyer, A., “Active Gurney Flaps: Their Application in a Rotor Blade Centrifugal Field,” *Journal of Aircraft*, Vol. 51, No. 2, Mar.-Apr. 2014, pp. 473–489.
- [35] Zanotti, A. and Gibertini, G., “Experimental investigation of the dynamic stall phenomenon on a NACA 23012 oscillating aerofoil,” *Proceedings of the Institution of Mechanical Engineers, Part G: Journal of Aerospace Engineering*, Vol. 227, No. 9, 2013, pp. 1375–1388.
- [36] Zanotti, A., Grassi, G., and G., G., “Experimental investigation of a trailing edge L-shaped tab on a pitching airfoil in deep dynamic stall conditions,” *Part G: Journal of Aerospace Engineering*, No. 12, Dec. 2013.
- [37] Motta, V. and Quaranta, G., “Linear Reduced-Order Model for Unsteady Aerodynamics of an L-Shaped Gurney Flap,” *Journal of Aircraft*, 2015, doi: 10.2514/1.C033099.
- [38] Liu, T. and Montefort, J., “Thin-Airfoil Theoretical Interpretation for Gurney Flap Lift Enhancement,” *Journal of Aircraft*, Vol. 44, No. 2, Mar.-Apr. 2007, pp. 667–671.
- [39] Kinzel, M., *Miniature Trailing-Edge Effectors for Rotorcraft Applications*, Master’s thesis, Aug. 2004.
- [40] Hariharan, N. and Leishman, J. G., “Unsteady Aerodynamics of a Flapped Airfoil in Subsonic Flow by Indicial Concepts,” *Journal of Aircraft*, Vol. 33, No. 5, Sep.-Oct. 1996, pp. 855–868.
- [41] Vieira, B., Kinzel, M., and Maughmer, M., “Unsteady Aerodynamics of Miniature Trailing-Edge Effectors Based on Indicial Methods,” *49th AIAA Aerospace Sciences Meeting, AIAA Paper 2011-1049*, Jan. 2011.
- [42] Johnson, W., “Self-Tuning Regulators for Multicyclic Control of Helicopter Vibrations,” Tech. rep., NASA TP, 1996.
- [43] Richter, K. and Rosemann, H., “Experimental investigation of trailing-edge devices at transonic speeds,” *The Aeronautical Journal*, No. 2621, April 2002, pp. 183–193.
- [44] Li, Y., Wang, J., and Hua, J., “Experimental investigations on the effects of divergent trailing edge and Gurney flaps on a supercritical airfoil,” *Aerospace Science and Technology*, No. 11, Dec. 2006, pp. 91–99.
- [45] Motta, V., *Computational fluid dynamic analysis of a L-shaped Gurney flap for vibration control*, Ph.D. thesis, 2015.
- [46] Küssner, H. and Schwarz, L., “The oscillating wing with aerodynamically balanced elevator,” TM 991, NACA, 1941, Translated from Luftfahrtforschung, vol. 17, pp. 337–354, 1940.
- [47] Fung, Y., *Theory of Aeroelasticity*, John Wiley and Sons, Inc., New York, 1955.
- [48] Kinzel, M., Maughmer, M., and Lesieutre, G., “Numerical Investigation of Miniature Trailing-Edge Effectors on Static and Oscillating Airfoils,” 43rd AIAA Aerospace Sciences Meeting and Exhibit, Reno, NV, 10–13 January 2005.
- [49] Leishman, J. G., *Principles of Helicopter Aerodynamics*, Cambridge University Press, 2006.
- [50] Bisplinghoff, R., Ashley, H., and Halfman, R., *Aeroelasticity*, Addison-Wesley Publishing Company, Cambridge, Mass., 1955.
- [51] Johnson, W., *Rotorcraft Aeromechanics*, Cambridge University Press, New York, 2013.
- [52] Theodorsen, T., “General Theory of Aerodynamic Instability and the Mechanism of Flutter,” TR 496, NACA, 1935.
- [53] Patt, D., Liu, L., Chandrasekar, J., S., B. D., and Friedmann, P. P., “Higher-Harmonic-Control Algorithm for Helicopter Vibration Reduction Revisited,” *Journal of Guidance, Control, and Dynamics*, Vol. 28, No. 5, 2005, pp. 918–930.
- [54] Milgram, J. and Chopra, I., “Helicopter Vibration Reduction with Trailing Edge Flaps,” *36th AIAA/ASME/ASCE/AHS/ASC Structures, Structural Dynamics and Materials Conference, New Orleans, LA*, 10–12 April 1995.
- [55] Lemmens, Y., Erdelyi, H., and Olbrechts, T., “Design Study of an Active Gurney Flap System for Helicopter Rotor Blades,” *28th International Congress of the Aeronautical Sciences, Brisbane, AUS*, 23–28 September 2012.



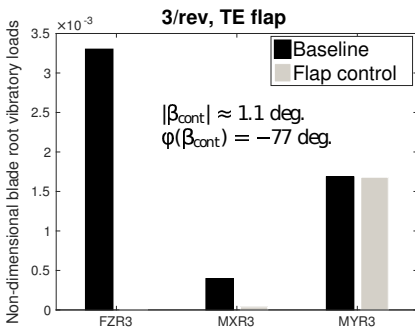
(a) 2/rev, control with the L-tab



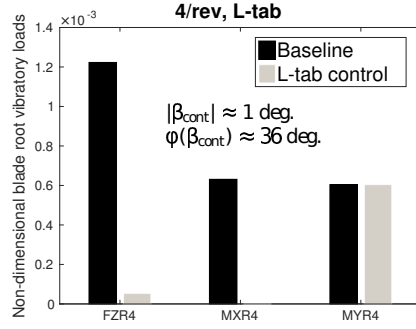
(b) 2/rev, control with the TE flap



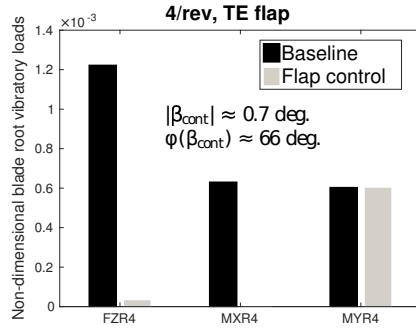
(c) 3/rev, control with the L-tab



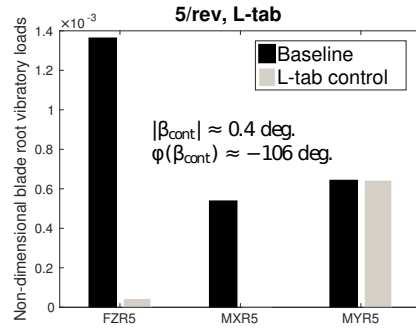
(d) 3/rev, control with the TE flap



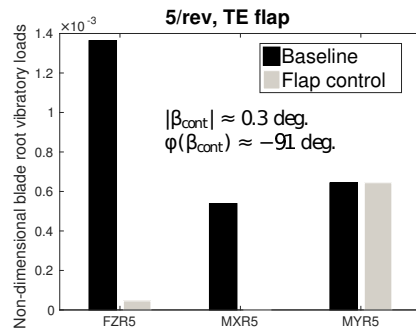
(a) 4/rev, control with the L-tab



(b) 4/rev, control with the TE flap



(c) 5/rev, control with the L-tab



(d) 5/rev, control with the TE flap

Figure 12: Rotating frame blade root 2/rev and 3/rev harmonic components of vertical force (FZ), bending (MX) and pitching (MY) moments with and without the addition of the movable device, controlled with the HHC approach;  $\mu = 0.2$ .

Figure 13: Rotating frame blade root 4/rev and 5/rev harmonic components of vertical force (FZ), bending (MX) and pitching (MY) moments with and without the addition of the movable device, controlled with the HHC approach;  $\mu = 0.2$ .

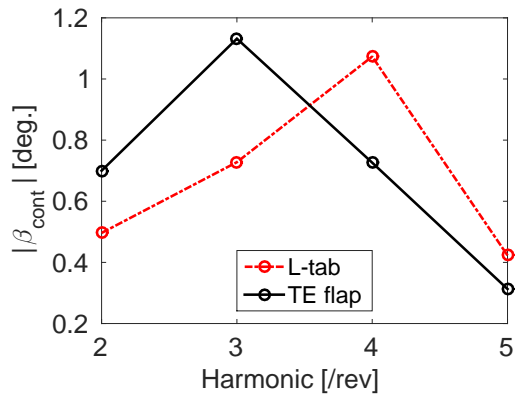


Figure 14: Amplitude of the HHC computed control inputs versus the minimized harmonic. The results attained for both the L-tab and the TE flap are reported.